RSC Advances

ROYAL SOCIETY OF CHEMISTRY

www.rsc.org/advances

Fabrication of a smooth, large-grained $Cu(In,Ga)Se_2$ thin film using a $Cu/(In,Ga)_2Se_3$ stacked precursor at low temperature for CIGS solar cells

Gwang Sun Jung, Sun Hong Mun, Donghyeop Shin, R. B. V. Chalapathy, Byung Tae Ahn*, and Hyuksang Kwon*

Department of Materials Science and Engineering, Korea Advanced Institute of Science and Technology, 291 Daehak-ro, Yuseong-gu, Daejeon 305-701, Republic of Korea

*Co-corresponding authors: btahn@kaist.ac.kr, hskwon@kaist.ac.kr

Abstract

$Cu(In,Ga)Se_2$ (CIGS) thin films used for commercial CIGS solar cells were fabricated from Cu-Ga-In metal precursors; they contained large voids at the CIGS/Mo interface and their surface was rather rough due to large volume expansion. To solve these problems, we employed a $Cu/(In,Ga)_2Se_3$ stacked precursor, in which the pre-existing Se could reduce the volume expansion during CIGS formation. With the pre-contained Se in the precursor, a uniform and void-free CIGS film with good adhesion was formed. SEM morphology revealed that a liquid phase was generated at 400°C by the reaction of Cu and $(In,Ga)_2Se_3$ under Se deficient conditions even though the melting point of Cu and $(In,Ga)_2Se_3$ are much higher. A large-grained CIGS film can be formed as low as 450°C with the help of liquid phase formation and we proposed the reaction mechanism. The film was applied to CIGS solar cells to achieve 13.5% efficiency without AR coating.

Keywords

$Cu(In,Ga)Se_2$, $Cu/(In,Ga)_2Se_3$, stacked precursor, liquid phase, low-temperature reaction

1. Introduction

$Cu(In,Ga)Se_2$ (CIGS) is one of the most promising absorber materials for thin film solar cells due to its high absorption coefficient of about 10^5 cm^{-1} and easy band-gap adjustment [1,2]. After crystal $CuInSe_2$ (CIS) realized the efficiency of 12% in 1974 [3], CIS-based solar cell technology has developed steadily to satisfy the electrical power generation demand. At present, the highest efficiency of polycrystalline thin-film CIGS solar cells is 20.8% by a three-stage process [4] and that of CIGS module efficiency is 14.6% in the total area of 1,228 m^2 by selenization and sulfurization [5]. For commercial fabrication, a two-stage process consisting of the deposition of metal precursor and the annealing of the precursor in H_2Se or H_2S gas is more attractive than in-situ co-evaporation where Cu, In, Ga and Se are evaporated. The advantage of the two-stage process is fast and achieves a uniform deposition of the precursor over a large area [6-8]. However, the selenization is conducted with H_2Se gas which is highly toxic and requires an additional safety facility. In addition, the adhesion of CIGS to Mo back-contact is poor because of stress built-up by volume expansion [9] and void formation at the CIGS/Mo interface by out diffusion of metal atoms from the Mo surface [10,11].

As alternative Se sources, Se pellets [12,13] or metal-organic sources [14] were used instead of H_2Se gas, but the interface void problem could not be easily solved. To avoid void formation, CIGS targets that already contained Se was employed [15]. However, the grain growth of the CIGS precursor by annealing because of high melting point of CIGS phase and cell performance was not improved [16-18]. To increase grain size of CIGS film, $CuSe/(In,Ga)_2Se_3$ precursor was suggested by using peritectic reaction of CuSe + excess Se(*l*)[19,20]. Excess Se atmosphere can increase the grain size of CIGS film [21]. To improve the cell performance, CIGS was grown with an Se-rich atmosphere in the both evaporation and two-stage processes, so the Se flux, the

criterion for the Se supply, plays an important role for CIGS grain growth [22,23]. Meanwhile, Kim et al. [24] reported that the CIGS is recrystallized by a residual Cu-Ga intermetallic phase during the Ar annealing step after the partial selenization step. The Cu-Ga intermetallic phase diffused to the grain boundary of CIGS from the Mo interface and induced the recrystallization of CIGS. So far, there has been little progress in the technology that can remove the voids at the CIGS/Mo interface and achieve large CIGS grains at the same time in the two-stage process, which is useful for large-area application.

In this paper, we propose a process technology that can reduce voids at the CIGS/Mo interface and increase CIGS grains at the same time. For that purpose, a precursor that contains Se is necessary. We selected an $(In,Ga)_2Se_3$ layer on Mo as a Se containing precursor. Since $(In,Ga)_2Se_3$ is the phase employed in the co-evaporation process, the phase has no chemical reaction with Mo. Then a Cu layer was deposited on the $(In,Ga)_2Se_3$ layer as for the precursor for CIGS film formation by the reaction of Cu and $(In,Ga)_2Se_3$. We investigated the reaction path of the Cu/$(In,Ga)_2Se_3$ precursor during ramping and found that a liquid phase was formed at as low as 400^{o}C and enhanced the grain growth of the CIGS film.

2. Experimental

CIGS thin films were grown by a two-stage process. In the first stage, a precursor was deposited with a Cu/$(In,Ga)_2Se_3$ stacked structure on Mo-coated soda lime glass (SLG) substrates. The $(In,Ga)_2Se_3$ films were deposited by a Knudsen cell (effusion cell) with the In, Ga and Se elemental sources. The thickness of the $(In,Ga)_2Se_3$ films was about 1.7 μm and the substrate temperature was maintained at 360ºC. Then the Cu layer was sputter-deposited on the $(In,Ga)_2Se_3$ layer at room temperature. The power density of the Cu deposition was 45.6 W/cm^2

with a DC magnetron sputtering system and the working pressure was 3 mTorr using Ar gas. The thickness of the Cu films was about 300 nm. Figure 1 shows the SEM surface and cross-section images of (a) the $(In,Ga)_2Se_3$ layer and (b) the Cu/$(In,Ga)_2Se_3$ stacked precursor on a Mo-coated SLG substrate. The surface image of the $(In,Ga)_2Se_3$ layer shows that the grain size of the $(In,Ga)_2Se_3$ is about 1 μm and that of the Cu layer in Fig. 1b shows that the Cu was aggregated to follow the morphology of $(In,Ga)_2Se_3$ grains. Voids are seen between Cu agglomerates. Figure 2 shows the XRD patterns of $(In,Ga)_2Se_3$ layer and Cu/$(In,Ga)_2Se_3$ precursor on Mo substrate. The crystal structure of $(In,Ga)_2Se_3$ was randomly oriented γ-$(In,Ga)_2Se_3$ phase [25] and the XRD pattern of Cu/$(In,Ga)_2Se_3$ precursor shows that only Cu and γ–$(In,Ga)_2Se_3$ exist in the precursor.

In the second stage, the precursor was ramped to a specific temperature without supplying Se. The base pressure of the vacuum system was below 2×10^{-6} Torr and the substrate was heated from room temperature with a 25 ºC/min heating speed. Selenization proceeded at 500ºC with various annealing times. The phase change of the precursors was investigated at the ramping temperatures of 200, 300, 350, 400, 450 and 500^{o}C.

To investigate the film morphology, field-emission scanning electron microscopy (FE-SEM, FEI Nova230) was used. The composition profiles of the films were investigated by energy dispersive X-ray spectroscopy (EDS) with 20 kV. To determine the phases in the films, X-ray diffraction (XRD, Rigaku D/Max-RC) and Raman spectroscopy (Horiba Jobin Yvon ARAMIS) were used. The XRD source was Cu Kα at 30 kV and 60 mA, and the Raman spectroscopy source was the 514 nm emission line of Ar ion laser. The elemental depth profile was determined by Auger electron spectroscopy (Perkin Elmer SAM4300). The CIGS solar cells were fabricated by an ordinary substrate structure with Al grid/ZnO:Al/i-ZnO/CdS/CIGS/Mo/SLG [26]. Selenization proceeded under optimized conditions. The J-V property of the solar cells (active

area 0.43 cm^2) was analyzed under AM 1.5 at room temperature.

3. Results and discussion

3.1 Ramping temperature effect on the morphology and phase

The morphology and phase of film during ramping were investigated with SEM images, XRD patterns, Raman spectra, and AES depth analysis at various ramping temperatures by ex-situ analysis. Cu/$(In,Ga)_2Se_3$ precursors on an Mo coated SLG substrate were annealed and cooled down as soon as the sample temperature reached a target temperature.

Figure 3 shows the SEM morphologies of the annealed films at the ramping temperatures of 300, 400, 450 and 500°C. The morphologies of the films at 100 and 200ºC were similar to that of the film at 300°C. At 350ºC, the apparent thickness of the Cu layer was reduced and the morphology of the bottom layer showed many twins. At 400°C, the shape of CIGS grains changed to small round grains and also very large round humps appeared on the CIGS surface. The large round humps on the CIS surface indicated those humps were in a liquid state. The generation of the liquid phase was a surprising result because both Cu and $(In,Ga)_2Se_3$ have much higher melting points than 400°C. The melting points of Cu and In_2Se_3 are 1085 and 890°C, respectively. The Cu/(In+Ga) and Ga/(In+Ga) ratios at a hump marked as point A were ~1.32 and ~ 0.26 by EDS, indicating that the hump was a metal alloy liquid. Note that the shape of the CIGS grains became round at this temperature due to the help of the metal alloy liquid.

At 450°C, the grain size of the CIGS phase increased to 1 μm and the large humps on the surface shown at 400°C disappeared. On the other hand, round grains with a 200-nm diameter appeared at the corners of the large CIGS grains. The Cu/(In+Ga) and Ga/(In+Ga) ratios at the 200-nm round grains near the CIGS surface marked as point B were 1.79 and 0.57, respectively.

Those ratios in the bulk (point C) were 1.47 and 0.52, respectively, by EDS analysis. At 500°C, the shape of the CIGS grains changed to a bamboo microstructure with about a 2 μm grain size and the Cu/(In+Ga) ratio was ~ 0.86 by AES analysis, but new small particles were observed on the top of the grains and the surface morphology became rough.

Figure 4 shows the XRD patterns of CIGS samples at various ramping temperatures, measured by (a) a coupled scan and (b) a 2θ scan with an initial theta of 2°. At 100°C, there were γ-$(In,Ga)_2Se_3$ (JCPDS 40-1407) and Cu (JCPDS 04-0836) layers. At 300ºC, the β-$(In,Ga)_2Se_3$ (JCPDS 40-1408) phase appeared and the γ-$(In,Ga)_2Se_3$ phase nearly disappeared. Further, a CIGS phase appeared at the surface of the precursor from the 2θ scan in figure 4b. At 350°C, β-$(In,Ga)_2Se_3$ disappeared and a CIGS phase appeared. A (In,Ga)Se (JCPDS 34-1431) phase as a new selenide phase also appeared.

At 400°C, the (220) peak intensity of the CIGS phase greatly increased (or sharpened), and a $Cu_9(In,Ga)_4$ (JCPDS 42-1476) phase was detected in addition to the (In,Ga)Se phase. As shown in the 2θ scan in figure 4b, there was a $Cu_9(In,Ga)_4$ phase on the film surface. At 450°C, the (112) peak intensity of the CIGS phase strongly increased and the $Cu_4(In,Ga)$ phase was detected. The (In,Ga)Se and $Cu_9(In,Ga)_4$ phases shown at 400°C disappeared. The $Cu_4(In,Ga)$ phase (JCPDS 42-1477) was found instead of $Cu_9(In,Ga)_4$ phases. At 500°C, the (In,Ga)Se phase reappeared as a round shape in addition to the CIGS phase and the Cu-(In,Ga) intermetallic phase disappeared.

Figure 5 shows Raman spectra of the samples at 400, 450 and 500°C ramping temperatures. Below 400°C, no signal was detected because the Cu top layer reflects the laser source. (In,Ga)Se and CIGS phases were observed at 400°C and only CIGS was observed at 450°C. A metallic alloy existing at 400 and 450°C was not detected because a laser cannot excite a metal

phase. At 500°C, CIGS, Cu_2Se and (In,Ga)Se phases were observed. It seen that, at a high temperature in a vacuum, Se is sublimated from the CIGS phase and the CIGS phase is dissociated into Cu_2Se and (In,Ga)Se phases. The InSe phase is a volatile phase and can be easily evaporated in a vacuum [27], so the surface of the CIGS become rough and Cu_2Se particles remained.

Figure 6 shows the AES depth profiles of Cu, In, Ga and Se at the ramping temperature of 300, 350, 400, 450 and 500°C. At 300°C, a CIGS layer was formed half way through the β-$(In,Ga)_2Se_3$ precursor layer by Cu diffusion. Note that Cu content was low but constant in the CIGS phase region. Since the Cu content is low, the CIGS phase existing at the surface seems to be a $Cu(In,Ga)_3Se_5$ phase. At 350°C, the Cu content is uniform throughout the $(In,Ga)_2Se_3$ precursor. This indicates that the $Cu(In,Ga)_3Se_5$ phase exists throughout the $(In,Ga)_2Se_3$ precursor layer and there is no $(In,Ga)_2Se_3$ phase. At 400°C, the Cu content was substantially increased in the bulk and the In content was significantly lower in the bulk. This is possibly due to the formation of a liquid phase. Note that the Ga content was not changed significantly while the In content was significantly changed. This suggests that the liquid formed at 400°C is mainly from In, not from Ga and liquid In reacts with Cu metal to form a liquid CuIn alloy. At the CIGS/Mo interface, the In content is high and the Cu content is low. The In content at the interface was initially high and was not lowered much at the interface. At 450°C, Cu almost dissolved into the bulk and the In content at the surface was slightly decreased, indicating that a liquid CuIn alloy was dissolved into the bulk layer. At 500°C, all the elements were uniform throughout the CIGS layer and the Cu/(In+Ga) ratio was 0.86. However, the Cu_2Se and (In,Ga)Se phases formed at the CIGS surface by the decomposition of CIGS in a vacuum at high temperature from XRD and Raman analysis.

Based on the analysis from SEM images, XRD patterns, Raman spectra, and AES depth profiles, the CIGS reaction path from the Cu/$(In,Ga)_2Se_3$ precursor at each ramping temperature is summarized in Table I.

Figure 7 is the schematic cross sectional view of the precursor reaction path at the ramping temperatures of 300, 350, 400, 450 and 500^{o}C. At 200^{o}C, γ-$(In,Ga)_2Se_3$ and β-$(In,Ga)_2Se_3$ phases coexist. At 300^{o}C, the $Cu(In,Ga)_3Se_5$ layer formed on the β-$(In,Ga)_2Se_3$ layer. At 350^{o}C, the $(In,Ga)_2Se_3$ layer was converted to a $Cu(In,Ga)_3Se_5$ layer. At 400^{o}C, a $Cu(In,Ga)Se_2$ layer formed and a liquid CuIn alloy formed on the surface. At that point, In moves out to the surface. The Cu atoms in CuIn(*l*) move into the CIGS bulk area. Much of the CuIn(*l*) stays at the CIGS surface. Small spherical grains appear at this temperature due to stress relaxation by the liquid phase. At 450^{o}C, the liquid CuIn moves into CIGS grain boundaries to fill open space generated by grain growth. The Cu content increased in the bulk. At this time grain size increased remarkably. The growth mechanism is Ostwald ripening with liquid-assisted grain growth where component elements move very fast through the liquid phase [24,28]. At 500^{o}C, the shape of the grain changed to a bamboo shape where the surface area grain was minimized.

3.2 Effect of selenization on the CIGS solar cell performance

After ramping to 500^{o}C, the samples were annealed in a vacuum chamber with Se supplied from an effusion cell. The pressure of the chamber while the Se was being supplied was below 2×10^{-6} Torr and the Se flux was 25 Å/s. Before selenization, the Cu/(In+Ga) ratio and Se content of the CIGS film were 0.86 and 47.3 at%, respectively. By the Se being supplied at 500^{o}C, the CIGS film composition ratio was optimized to Cu/(In+Ga) = 0.88-0.94, Ga/(In+Ga) = 0.31-0.34 and Se composition 50.1-51.0 at%.

Figure 8 shows the SEM surface images of the CIGS films annealed at 500^{o}C with the Se annealing times of 10, 20 and 30 min. After 10 min selenization, the shape of the CIGS grains changed to facetted from round in figure 3, suggesting that the open spaces among the grains were filled by selenization. A pinhole (marked as D) that crossed from surface to Mo was seen in the cross section in figure 8. After 20 min selenization, the surface morphology was similar to that of the CIGS film selenized for 10 min and there were more pores on the surface. However, the grains were more closely packed in the cross section image. After 30 min selenization, there were more voids at the surface and the surface became rough due to surface re-growth [22]. No void was observed at the CIGS/Mo interface, which indicated that adhesion between CIGS and Mo is good. It is seen that the pre-existing Se in the precursor suppressed the void formation at the CIGS/Mo interface.

Figure 9 shows the J-V curves of the CIGS solar cells that employed the selenized CIGS films at 500^{o}C for 10, 20 and 30 min. The photovoltaic parameters of the cells, the open circuit voltage (V_{oc}), short circuit current (J_{sc}), fill factor (FF), series resistance (R_s), shunt resistance (R_{sh}), and reverse saturation current (J_o), are summarized in Table II. With the selenization times of 10, 20 and 30 min, the cell efficiency increased from 8.62 to 10.8 and decreased to 9.7%. The V_{oc}, J_{sc}, and FF values were much lower than a referenced cell conventionally prepared by a three-stage evaporation process.

AES depth profiles of Cu, In, Ga, and Se in the CIGS film prepared at 500^{o}C for 20 min selenization are shown in figure 10a. In and Ga content was uniform right after 500^{o}C ramping (Fig. 6). However, after selenization, In was accumulated and Ga was depleted at the CIGS surface. As a result, V_{oc}, J_{sc}, and FF were low compared to the reference cell. The depth of In accumulation and Ga depletion near the surface in our sample was much more shallow than that

of In accumulation and Ga depletion in the CIGS film prepared by direct selenization of metal precursors [8], so surface depletion of Ga could be controlled by an additional Ga supply on the surface of the precursor or S treatment during annealing or additional Ga supply after CIGS formation.

Ga was supplied to the surface of the CIGS film selenized at 500°C for 20 min by evaporation at 360°C for 2 min. The J-V curve of the CIGS solar cell with surface treatment is shown in figure 9. Its photovoltaic parameters are also shown in figure 9 and listed in Table II. With the increase of Ga treatment, the open-circuit voltage and short-circuit current increased. As a result, the efficiency increased from 10.8% to 13.5%. The In and Ga profile after surface Ga treatment is shown in figure 10b. The AES depth profile indicated that Ga content is not high enough to achieve a higher V_{oc}. The result demonstrated that a higher performance device can be obtained by controlling the Ga content at the CIGS surface. Pre-deposition of Ga on the Cu/$(In,Ga)_2Se_3$ precursor or sulfurization after CIGS formation could help to further improve the cell performance.

5. Conclusions

A Cu/$(In,Ga)_2Se_3$ stacked precursor instead of a metal precursor was employed to minimize volume expansion during the selenization process so that void formation at the CIGS/Mo interface could be suppressed. Morphology changes and phase changes with various ramping temperatures were investigated. The SEM images showed that a liquid phase was formed at 400°C and a small spherical-shaped CIGS phase formed at the same time. A CIGS film with large grains was achieved at 450°C and a CIGS film with a bamboo microstructure was obtained at 500°C. The surface of the CIGS film was uniform and no voids formed at the CIGS/Mo

interface.

From the analysis of SEM images, XRD patterns, Raman spectra, and AES depth profiles, the following reaction was observed. Below 350°C, Cu diffused into $(In,Ga)_2Se_3$ and formed a Cu-deficient $Cu(In,Ga)_3Se_5$ phase. At 400°C, Cu and $Cu(In,Ga)_3Se_5$ reacted to form a Cu(In,Ga)Se2 phase and a liquid CuIn alloy phase. At that temperature, the shape of CIGS grains became round. The Cu content in the CIGS bulk substantially increased and the In content in bulk strongly decreased. Above 450°C, grain size increased fast due to the existence of a liquid CuIn alloy phase.

The CIGS film annealed at 500°C for 20 min in a Se atmosphere showed a smooth surface with little pores between grains. Voids at the CIGS/Mo interface were suppressed by our Se-containing precursor. Further annealing caused large pores and crevices between grains. The CIGS film selenized at 500°C for 20 min showed an In-rich and Ga-deficient surface. With an increasing Ga content at the CIGS surface by Ga supply through vacuum evaporation, the cell performance increased to 13.5% without AR coating. Further improvement in cell efficiency is expected by increasing Ga content at the CIGS surface.

Acknowledgements

This work was supported by the Center for Inorganic Photovoltaic Materials (No. 2012-0001167), and the Priority Research Center Program (2011-0031407) funded by the Korean Ministry of Education, Science and Technology.

References

1. M. Gossla and W. N. Shafarman, Five-source PVD for the deposition of $Cu(In_{1-x}Ga_x)(Se_{1-y}S_y)_2$, *Thin Solid Films*, 2005, **480**, 33-36.

2. U. Parihar, K. Sreenivas, J. R. Ray, C. J. Panchal, N. Padha and B. Rehani, Influence of substrate temperature on structural, optical, and electrical properties of flash evaporated $CuIn_{0.81}Al_{0.19}Se_2$ thin films, *Mater. Chem. Phys.*, 2013, **139**, 270-275.

3. S. Wagner, J. L. Shay and H. M. Kasper, The p-$CuInSe_2$/n-CdS heterodiode : photovoltaic detector, solar cell and light emitting diode, *J. de Physique*, 1975, **36**, 101-104.

4. P. Jackson, D. Hariskos, R. Wuerz, W. Wischmann and M. Powalla, Compositional investigation of potassium doped $Cu(In,Ga)Se_2$ solar cells with efficiencies up to 20.8%, *phys. Status Solidi-R*, 2014, **8**, 219-222.

5. K. Kushiya, CIS-based thin-film PV technology in solar frontier K.K, *Sol. Energ. Mat. Sol. Cells*, 2014, **122**, 309-313.

6. R. Kamada, W. N. Shafarman and R. W. Birkmire, $Cu(In,Ga)Se_2$ film formation from selenization of mixed metal/metal–selenide precursors, *Sol. Energ. Mat. Sol. Cells*, 2010, **94**, 451-456.

7. A. Cho, S. J. Ahn, J. H. Yun, J. H. Gwak, H. J. Song and K. H. Yoon, A hybrid ink of binary copper sulfide nanoparticles and indium precursor solution for a dense $CuInSe_2$ absorber thin film and its photovoltaic performance, *J. Mater. Chem.*, 2012, **22**, 17893-17899.

8. M. S. Kim, R. B. V. Chalapathy, K. H. Yoon and B. T. Ahn, Grain growth enhancement and Ga distribution of $Cu(In_{0.7}Ga_{0.3})Se_2$ film using Cu_2Se layer on Cu-In-Ga metal precursor, *J. Electrochem. Soc.*, 2010, **157**, B154-B158.

9. A. Gupta and S. Isomura, Precursor modification for preparation of CIS films by selenization technique, *Sol. Energ. Mat. Sol. Cells*, 1998, **53**, 385-401.

10. S. Y. Hsiao, P. C. Yang, H. C. Ni, K. Y. Yen, C. H. Chiu, P. S. Lin, H. J. Chen, C. H. Wu, S. C. Liang, G. Y. Ni, F. W. Jih, C. D. Chiang and J. R. Gong, Characteristics of $Cu(In,Ga)Se_2$ films prepared by atmospheric pressure selenization of Cu-In-Ga precursors using Ditert-Butylselenide as Se Source, *J. Electrochem. Soc.*, 2012, **159**, H378-H383.

11. D. J. Schroeder, G. D. Berry and A. A. Rockett, Gallium diffusion and diffusivity in $CuInSe_2$ epitaxial layers, *Appl. Phys. Lett.*, 1996, **69**, 4068-4070.

12. F. B. Dejene, The structural and material properties of $CuInSe_2$ and $Cu(In,Ga)Se_2$ prepared by selenization of stacks of metal and compound precursors by Se vapor for solar cell applications, *Sol. Energ. Mat. Sol. Cells*, 2009, **93**, 577-582.

13. W. Li, Y. Sun, W and Liu, L. Zhou, Fabrication of $Cu(In,Ga)Se_2$ thin films solar cell by selenization process with Se vapor, *Sol. Energy*, 2006, **80**, 191–195.

14. M. Uchikoshi and S. Shirakata, Control of grain in $Cu(In,Ga)Se_2$ thin films prepared by selenization method using Diethylselenide, *Jpn. J. Appl. Phys.*, 2012, **51**, 10NC20.

15. Y. C. Lin, J. H. Ke, W. T. Yen, S. C. Liang, C. H. Wu and C. T. Chiang, Preparation and characterization of $Cu(In,Ga)(Se,S)_2$ films without selenization by co-sputtering from $Cu(In,Ga)Se_2$ quaternary and In_2S_3 targets, *Appl. Surf. Sci.*, 2011, **257**, 4278-4284.

16. J. H. Shi, Z. Q. Li, D. W. Zhang, Q. Q. Liu, Z. Sun and S. M. Huang, Fabrication of Cu(In, Ga)Se_2 thin films by sputtering from a single quaternary chalcogenide target, *Prog. Photovoltaics Res. Appl.*, 2011, **19**, 160-164.

17. J. A. Frantz, R. Y. Bekele, V. Q. Nguyen, J. S. Sanghera, A. Bruce, S. V. Frolov, M. Cyrus and I. D. Aggarwal, $Cu(In,Ga)Se_2$ thin films and devices sputtered from a single target without additional selenization, *Thin Solid Films*, 2011, **519**, 7763-7765.

18. A. J. Zhou, D. Mei, X. G. Kong, X. H. Xu, L. D. Feng, X. Y. Dai, T. Gao and J. Z. Li, One-

step synthesis of $Cu(In,Ga)Se_2$ absorber layers by magnetron sputtering from a single quaternary target, *Thin Solid Films*, 2012, **520**, 6068-6074.

19. J. Koo, S. C. Kim, H. Park and W. K. Kim, $Cu(InGa)Se_2$ thin film photovoltaic absorber formation by rapid thermal annealing of binary stacked precursors, *Thin Solid Films*, 2011, **520**, 1484-1488.

20. X. L. Zhu, Y. M. Wang, Z. Zhou, A. M. Li, L. Zhang and F. Q. Huang, 13.6%-efficient $Cu(In,Ga)Se_2$ solar cell with absorber fabricated by RF sputtering of $(In,Ga)_2Se_3$ and CuSe targets, *Sol. Energ. Mat. Sol. Cells*, 2013, **113**, 140-143.

21. L. L. Kerr, S. S. Li, S. W. Johnston, T. J. Anderson, O. D. Crisalle, W. K. Kim, J. Abushama and R.N. Noufi, Investigation of defect properties in $Cu(In,Ga)Se_2$ solar cells by deep-level transient spectroscopy, *Solid State Electron.*, 2004, **48**, 1579-1586.

22. K. H. Kim, K. H. Yoon, J. H. Yun and B. T. Ahn, Effects of Se flux on the microstructure of $Cu(In,Ga)Se_2$ thin film deposited by a three-stage co-evaporation process, *Electrochem. Solid Sate Lett.*, 2006, **9**, A382-A385.

23. J. Kessler, C. Chityuttakan, J. Lu, J. Schöldström and L. Stolt, $Cu(In,Ga)Se_2$ thin films grown with a Cu-poor/rich/poor sequence: growth model and structural considerations, *Prog. Photovoltaics Res. Appl.*, 2003, **11**, 319-331.

24. K. H. Kim, G. M. Hanket, T. Huynh and W. N. Shafarman, Three-step $H_2Se/Ar/H_2S$ reaction of Cu-In-Ga precursors for controlled composition and adhesion of $Cu(In,Ga)(Se,S)_2$ thin films, *J. Appl. Phys.*, 2012, **111**, 083710.

25. S. Chaisitsak, A. Yamada and M. Konagai, Preferred orientation control of $Cu(In_{1-x}Ga_x)Se_2$ ($x\approx0.28$) thin films and its influence on solar cell characteristics, *Jpn. J. Appl. Phys.*, 2002, **41**, 507.

26. D. H. Shin, J. H. Kim, Y. M. Shin, K. H. Yoon, E. A. Al-Ammar and B. T. Ahn, Improvement of the cell performance in the ZnS/Cu(In,Ga)Se_2 solar cells by the sputter deposition of a bilayer ZnO: Al film, *Prog. Photovoltaics Res. Appl.*, 2013, **21**, 217-225.

27. C. Chatillon, Critical analysis of the thermodynamic properties of the In-Se gaseous and solid phases, *J. Cryst. Growth*, 1993, **129**, 297-311.

28. J. O. Thompson, M. D. Anderson, T. Ngai, T. Allen and D. C. Johnson, Nucleation and growth kinetics of co-deposited copper and selenium precursors to form metastable copper selenides, *J. Alloy. Compd.*, 2011, **509**, 9631-9637.

List of figures

Figure. 1. SEM surface and cross-sectional images of the (a) $(In,Ga)_2Se_3$/Mo and (b) Cu/$(In,Ga)_2Se_3$/Mo precursor layer.

Figure. 2. XRD patterns of the (a) $(In,Ga)_2Se_3$ layer and (b) Cu/$(In,Ga)_2Se_3$ precursor on the Mo substrate; 1. γ-$(In,Ga)_2Se_3$, 2. Cu.

Figure. 3. SEM surface and cross-sectional images of Cu/$(In,Ga)_2Se_3$ precursors at ramping temperatures of 300, 350, 400, 450, and 500°C with a ramping rate of 25 °C/min.

Figure. 4. XRD patterns of the Cu/$(In,Ga)_2Se_3$/Mo precursors ramped at various temperatures with (a) coupled scans and (b) 2θ scans with the incident beam angle of 2°; 1. γ-$(In,Ga)_2Se_3$, 2. Cu, 3. β-$(In,Ga)_2Se_3$, 4. $Cu(In,Ga)_3Se_5$ (β-CIGS), 5. $Cu(In,Ga)Se_2$ (α-CIGS), 6. (In,Ga)Se, 7. $Cu_9(In,Ga)_4$, 8. $Cu_4(In,Ga)$.

Figure. 5. Raman spectra of Cu/$(In,Ga)_2Se_3$ precursors ramped at various temperatures with a ramp rate of 25 °C/min; 1. (In,Ga)Se, 2. $Cu(In,Ga)Se_2$ (α-CIGS), 3. Cu_2Se.

Figure. 6. AES depth-profiles of Cu/$(In,Ga)_2Se_3$ precursors ramped at various temperatures with a ramp rate of 25 °C/min.

Figure. 7. Schematic reaction models of Cu/$(In,Ga)_2Se_3$ precursors ramped at various temperatures with a ramp rate of 25 °C/min.

Figure. 8. SEM surface and cross-sectional images of the selenized films at 500°C for 10, 20 and 30 min in a Se atmosphere.

Figure. 9. J–V curves of a CIGS solar cells, employing CIGS films selenized at 500°C for 10 to 30 min in a Se atmosphere and a CIGS film with Ga surface treatment after 20 min selenization.

Figure. 10. AES depth profiles of CIGS films (a) selenized at 500°C for 20 min in a Se atmosphere and (b) treated in Ga after the selenization.

Table I. Summary of the reaction path of the Cu/$(In,Ga)_2Se_3$ precursor at various ramping temperatures.

Ramping temp. (^oC)	Reactions	Remark
200	γ-$(In,Ga)_2Se_3 \rightarrow \beta$-$(In,Ga)_2Se_3$ (114)	Phase transformation
300	Cu + β-$(In,Ga)_2Se_3 \rightarrow Cu(In,Ga)_3Se_5$	Solid-state reaction
400	3 Cu+ 2 $Cu(In,Ga)_3Se_5 \rightarrow$ 5 $Cu(In,Ga)Se_2$ +In(l) Cu + In(l) $\rightarrow$ CuIn(l)	Liquid formation
450	Liquid-assisted grain growth	Grain growth
500	$Cu(In,Ga)Se_2 \rightarrow Cu_2Se$ + (In,Ga)Se +Se(g)	Decomposition

Table II. Summary of device performance of CIGS solar cells that employed CIGS film prepared at 500°C with 10 to 30 min selenization. All the efficiencies were measured without AR coating.

Selenization time (min)	Eff. (%)	V_{oc} (V)	J_{sc} (mA/cm^2)	F.F.	R_s (Ωcm^2)	R_{sh} (Ωcm^2)
10	8.62	0.437	30.5	64.7	0.69	448
20	10.8	0.514	31.4	67.0	0.56	1530
30	9.72	0.487	30.5	65.5	0.81	980
20 and Ga treatment	13.5	0.555	36.0	67.5	0.67	2690
Three-stage process	17.6	0.650	36.5	74.2	0.37	8040

A table of contents entry

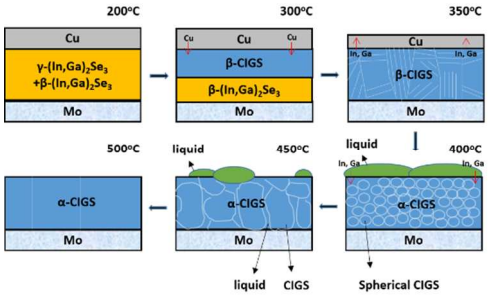

Grain growth of CIGS thin film assisted by liquid CuIn from Cu/$(In,Ga)_2Se_3$ stacked precursor.

Fig. 1

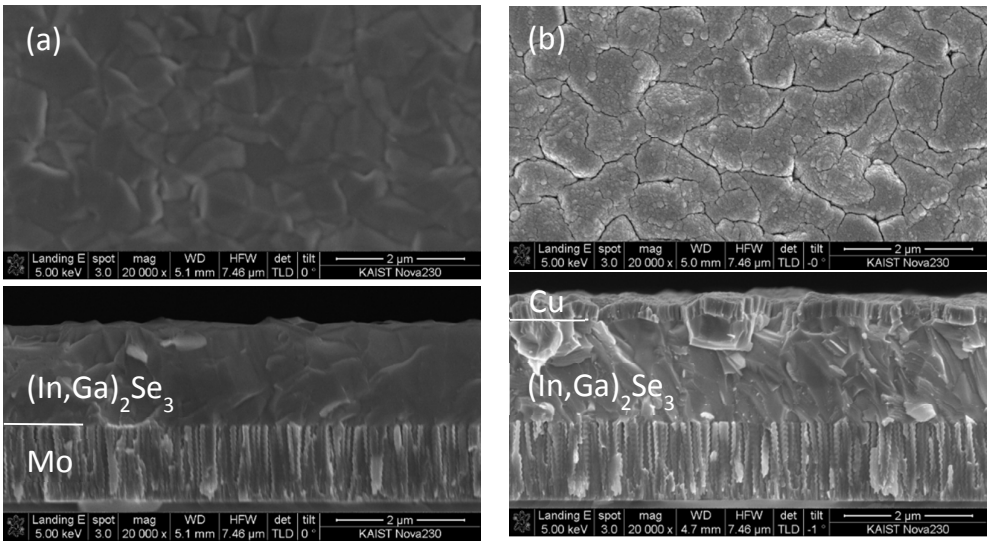

Fig. 2

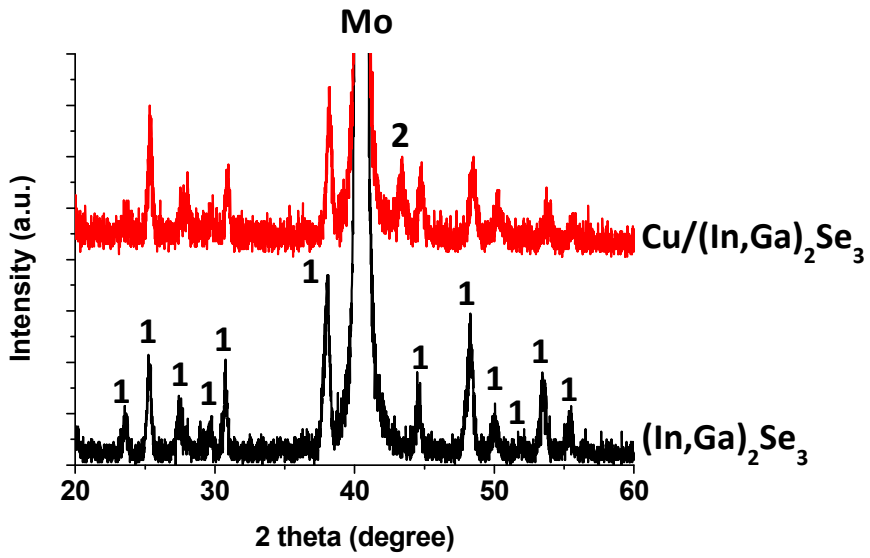

Fig. 3

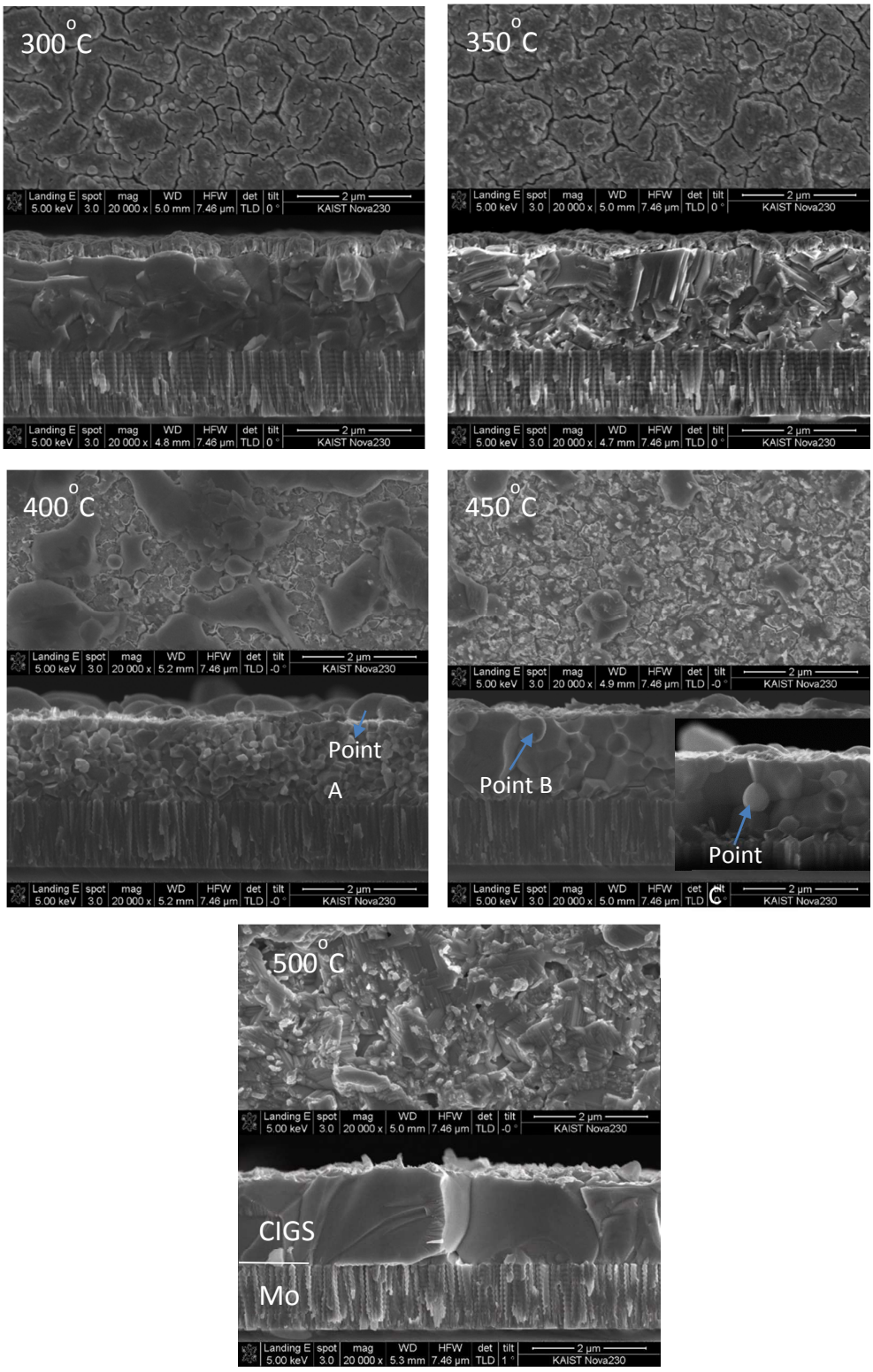

Fig. 4

(a)

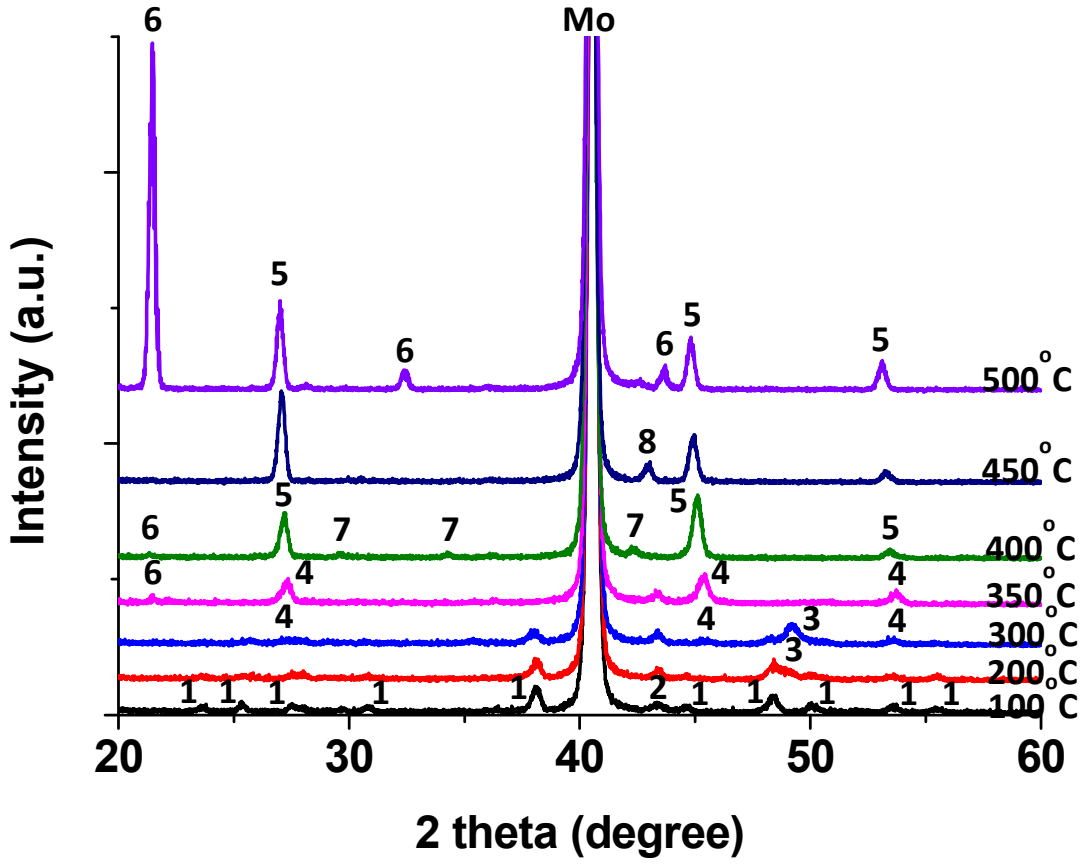

Fig. 4

(b)

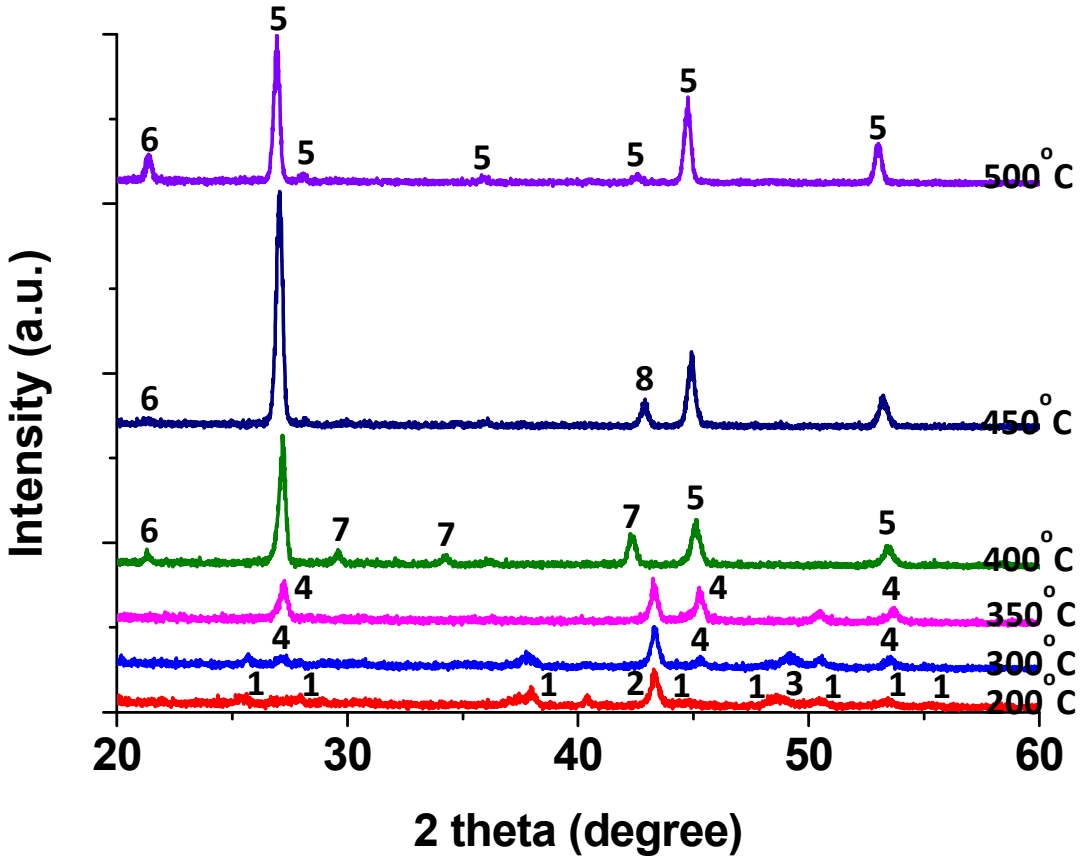

Fig. 5

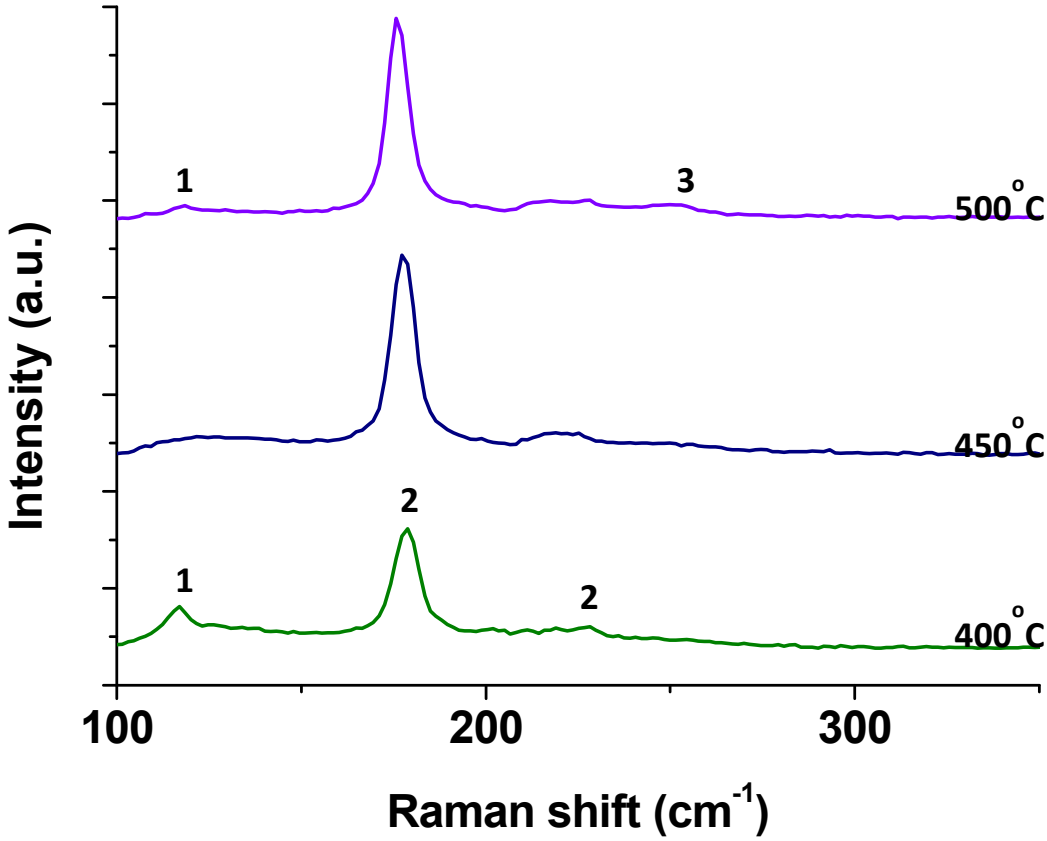

Fig. 6

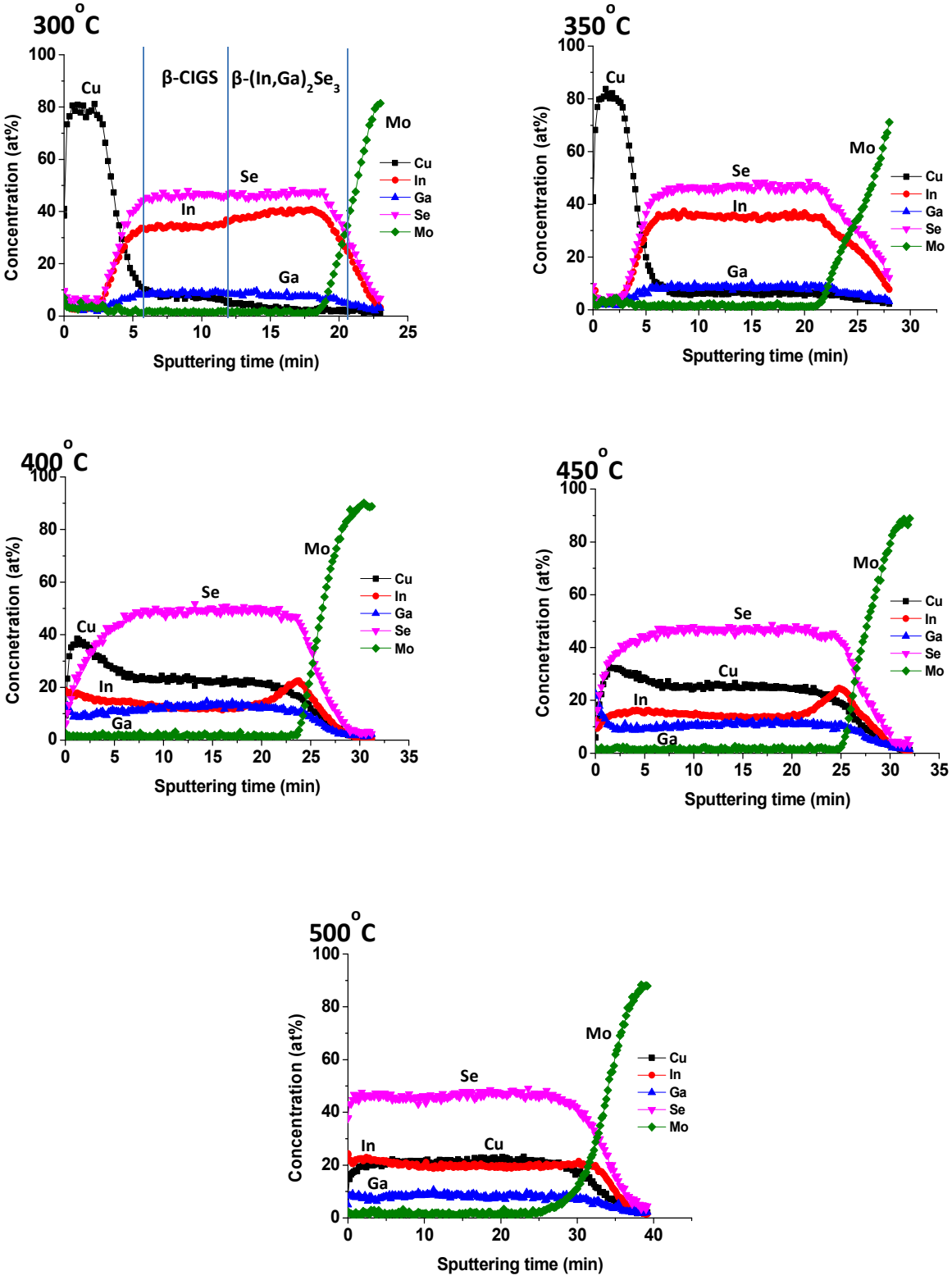

Fig. 7

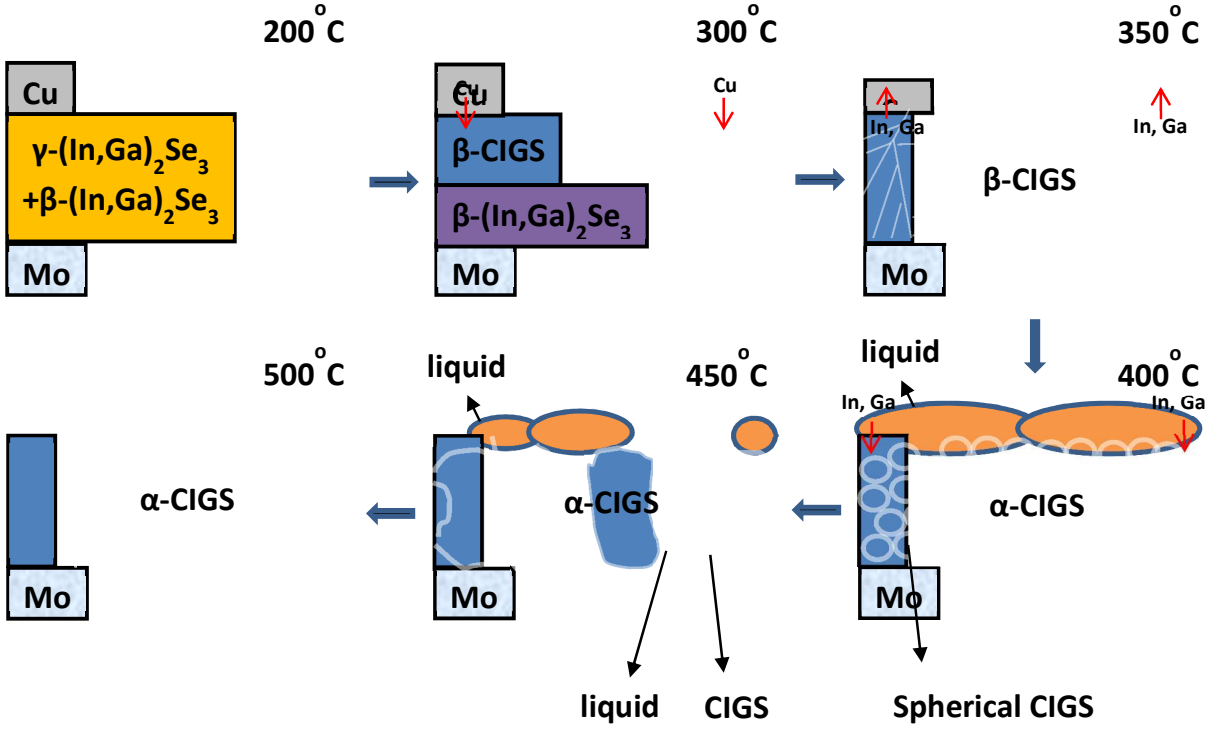

Fig. 8

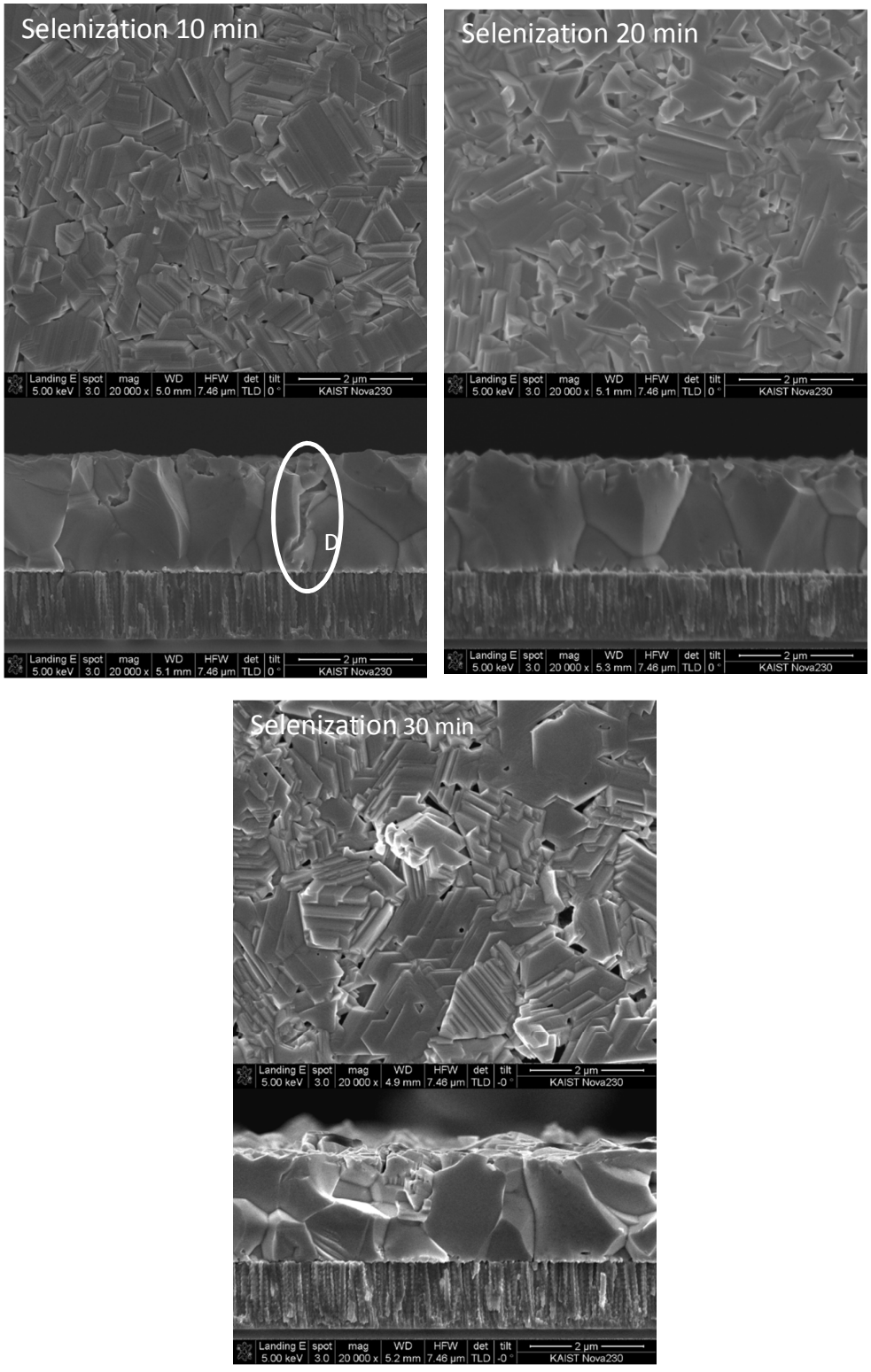

Fig. 9

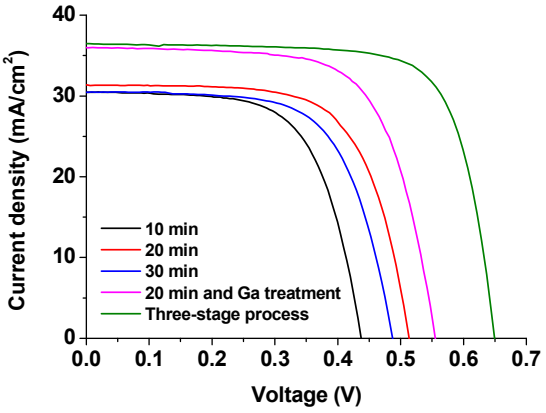

Fig. 10

(a)

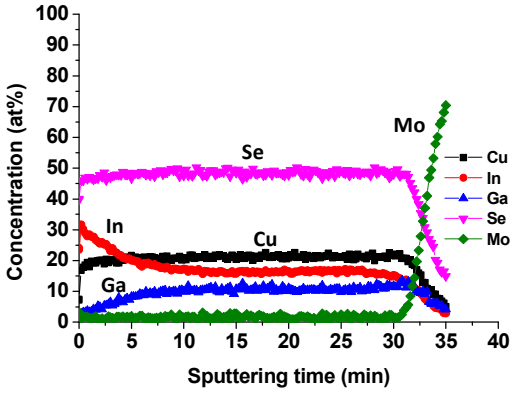

(b)